PROCEEDINGS OF SCIENCE

B^+ and Onia cross sections at 13 TeV at CMS

P. Ronchese on behalf of the CMS collaboration*
Dipartimento di Fisica e Astronomia
Università di Padova and INFN, I-35131 Padova, ITALY
E-mail: paolo.ronchese@pd.infn.it

Measurements of B^+ and quarkonium production cross sections provide essential information to understand QCD. This talk will show measurements of double-differential production cross sections vs. transverse momentum p_T and rapidity y at center-of-mass energy of $\sqrt{s} = 13$ TeV performed by the CMS experiment. Comparisons with expectations and results obtained at $\sqrt{s} =$ 7 TeV will be shown.

The International Conference on B-Physics at Frontier Machines - BEAUTY2018
6-11 May, 2018
La Biodola, Elba Island, Italy

*Speaker.

PoS(BEAUTY2018)012

1. Introduction

The motivations to study heavy flavour physics at CMS [1] include the probe of the underlying QCD processes, obtained by measuring b-hadron and quarkonium production cross sections. Such measurements are reference or ingredient for searches and measurements of rarer or new processes as well as a baseline for associated production of heavy flavour and other objects. The measurements of the production cross sections for B^+ mesons and ψ, Υ quarkonia from CMS at a center of mass energy $\sqrt{s} = 13$ TeV will be shown here.

2. The CMS experiment

The main components of the CMS experiment [1] are the tracker with pixels and microstrips, the electromagnetic and hadron calorimeters, and the muon detectors. Three different detectors are dedicated to muon trigger and detection, having the capability to perform a standalone reconstruction of muons. The match between the reconstruction from the tracker and the muon detectors can be conducted inside-out, that is more efficient at low tranverse momentum, or outside-in, that is more efficient at high p_T. The probability of wrongly identifying charged pions and kaons as muons is less than 1% and the momentum resolution ranges from 1% to 6% for muons up to 100 GeV.

Muons play an essential role in triggering events in the harsh LHC environment, characterized by a very high luminosity, while keeping the frequency inside a limited bandwidth. Triggers for B physics require the presence of two muons at least, possibly together with an additional track. The trigger system consists of a first level, based on a dedicated hardware taking a fast decision and giving a trigger rate of the order of ~ 100 kHz, followed by an higher level based on software performing full track reconstruction and giving a rate of ~ 1 kHz. Specific triggers have been developed for different analyses, applying cuts on muon and dimuon transverse momentum and rapidity, the presence of secondary vertices and their displacement from the interaction point, the dimuon mass and the angle formed by the dimuon momentum and the flight direction, given by the position of the secondary vertex relative to the collision point. In the first year of running at $\sqrt{s} = 13$ TeV LHC delivered an integrated luminosity $\mathscr{L} \sim 4$ fb^{-1}, and CMS recorded data corresponding to $\mathscr{L} \simeq 3.6$ fb^{-1}. For muon-based analyses an integrated luminosity $\mathscr{L} \simeq 2.7$ fb^{-1} was collected.

3. B^+ production

The measurement and study of beauty hadron production cross section at high energies provides new important tests of theoretical calculations [2, 3]. The B^+ production cross section was measured at the CMS experiment looking at the decay $B^+ \to J/\psi K^+$, followed by the decay $J/\psi \to \mu^+\mu^-$ [4]; charge conjugation states are implied here and in the following. The differential cross section versus transverse momentum or rapidity was measured in a rapidity range $|y_B| < 2.1$ and transverse momentum range 10 GeV $< p_{T,B} <$ 100 GeV, using a subsample of data collected in 2015 corresponding to an integrated luminosity $\mathscr{L} = 48.1$ pb^{-1}. The differential cross section was extracted from the signal yield in each bin dividing by the branching ratios $\mathscr{B}$, acceptance A,

efficiency ε, integrated luminosity and the bin width Δz, with $z = p_{T,B}, y_B$; an additional factor 2 was included to account for B charge symmetry, while the cross section for the production of B^+ only was quoted:

$$\frac{d\sigma(pp \to B^+X)}{dz} = \frac{n_{\rm sig}(z)}{2 \cdot \mathscr{B} \cdot A \cdot \varepsilon(z) \cdot \mathscr{L} \cdot \Delta z}.$$

Events were selected requiring the reconstruction of muons with hits in the strip tracker and pixel detector, the match of the extrapolated track with at least one segment reconstructed in the muon chambers, a transverse momentum $p_T > 4.2$ GeV and a pseudorapidity $|\eta| < 2.1$.

Candidate J/ψ mesons were reconstructed combining pairs of oppositely-charged muons having an invariant mass within ± 150 MeV of the nominal J/ψ mass, $p_{T,J/\psi} > 8$ GeV and a χ^2 probability of the vertex-fit larger than 10%. Both muons must be either within $|\eta| < 1.6$ or one of the muons must have $p_T > 11$ GeV.

Candidate B^+ mesons were reconstructed combining a J/ψ candidate with a charged track with $p_T > 1$ GeV; the track was assumed to be a kaon and the track fit was required to give $\chi^2/n_{\rm d.o.f.} < 5$. A kinematic fit was performed, constraining the dimuon mass to the nominal J/ψ mass; the three-track combination was required to be compatible with having a common vertex with a vertex-fit χ^2 probability larger than 10% and a reconstructed invariant mass $M_{J/\psi K}$ in the range $5 \div 6$ GeV. The transverse decay distance divided by its uncertainty was required to exceed 3.5 and the cosine of the angle between B^+ candidate momentum and the vector formed by the interaction point and the $\mu\mu K$ vertex in the transverse plane had to be greater than 0.99.

The B^+ invariant mass distribution was built in bins of transverse momentum and an unbinned maximum likelihood fit was performed; the signal was described with the sum of two gaussians and the background with an exponential plus an error function to describe the contribution of wrongly reconstructed decays of B^+ with additional particles in the final state. The invariant mass distribution for the inclusive sample in the total acceptance region is shown in Fig. 1.

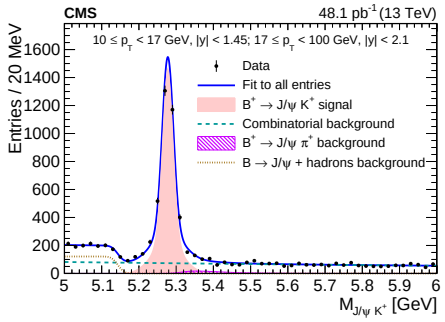

Figure 1: Invariant mass distribution of the full $B^\pm \to J/\psi K^\pm$ candidates sample: the solid curve shows the result of the fit, the shaded area represents the signal component, the dashed and dash-dotted curves represent the combinatorial and mis-reconstructed $B^\pm \to J/\psi K^\pm X$ background components, respectively [4].

The acceptance and efficiency were estimated with a sample of simulated events; trigger and muon reconstruction efficiency was estimated also in data selecting an inclusive J/ψ sample and applying a tag-and-probe method: the difference with the one obtained from the simulation was included in the systematic uncertainties.

To estimate other systematic uncertainties the mass modeling functions were changed; the rare decay $B^+ \to J/\psi\pi^+$ contribution was included in the fit; the uncertainty coming from bin to bin migration of events, due to finite resolution, was estimated by examining the generator information in the simulated samples. Uncertainties associated to the $p_{T,B}$ and y_B distributions used in the generation were evaluated with event-by-event weights determined from the differences between the distributions generated by PYTHIA and given by the FONLL calculations. The uncertainty on the B^+ lifetime was also included, the error on the integrated luminosity is 2.3% and the uncertainty on the branching ratios is 3.1%.

The differential cross section versus transverse momentum was integrated over $|y_B| < 1.45$, for 10 GeV $< p_T <$ 17 GeV, and $|y_B| < 2.1$ for 17 GeV $< p_T <$ 100 GeV. The differential cross section versus rapidity was integrated over 10 GeV $< p_T <$ 100 GeV, for $|y_B| <$ 1.45, and 17 GeV $< p_T <$ 100 GeV, for 1.45 $< |y_B| <$ 2.1.

The differential cross section versus transverse momentum and rapidity [4] is shown in Fig. 2, together with the results obtained at $\sqrt{s} = 7$ TeV [5] and the predictions from FONLL [2, 6, 7] and PYTHIA [8].

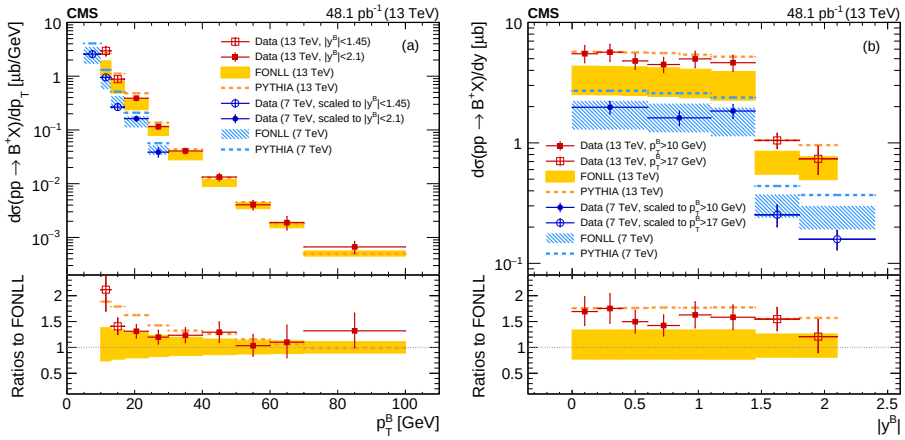

Figure 2: Differential cross section versus transverse momentum (left) and rapidity (right), compared with predictions from FONLL (boxes) and PYTHIA (dashed lines). The lower pads display the data over FONLL cross section ratios (dots) and the PYTHIA/FONLL ratios (dashed lines) [4].

The ratio of differential cross sections at $\sqrt{s} = 13$ TeV and $\sqrt{s} = 7$ TeV is shown in Fig. 3; the ratio has an interest in its own due to reduced sensitivity to scale uncertainty, that allows putting constraint to gluon PDF [9].

4. Quarkonium production

Quarkonium production can be described in two phases, with a perturbative generation of a quark-antiquark pair in a singlet or octet state followed by the hadronization producing a bound state, described by a long-distance matrix element [10–15]. Measurements at different energies allow for a test of this factorization; predictions are done performing different perturbative calculations for each different collision energy and using the same matrix element at all energies [16, 17].

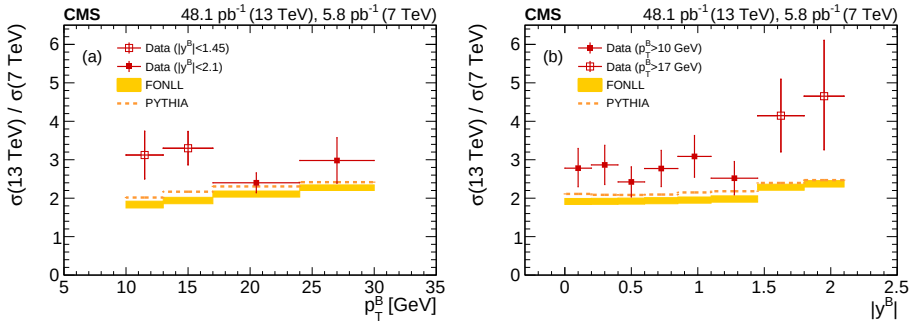

Figure 3: Ratios of differential cross section at $\sqrt{s} = 13$ TeV and $\sqrt{s} = 7$ TeV versus transverse momentum (left) and rapidity (right), compared with predictions from FONLL (boxes) and PYTHIA (dashed lines) [4].

Higher energies, with higher cross sections, allow for a measurement with an extended reach in transverse momentum, up to 120 GeV for rapidity up to 1.2, using the full available data sample collected in 2015 [18]. The product of double-differential cross section by decay branching ratio was extracted from the signal yield in each bin dividing by acceptance A, efficiency ε, integrated luminosity and the bin widths:

$$\mathscr{B}(Q\bar{Q} \to \mu^+\mu^-) \cdot \frac{d^2\sigma(pp \to Q\bar{Q}X)}{dp_T dy} = \frac{N_{Q\bar{Q}}(z)}{\mathscr{L} \cdot \Delta p_T \Delta y} \cdot \Big\langle \frac{1}{A(p_T, y) \cdot \varepsilon(p_T, y)} \Big\rangle.$$

The signal yield in each bin was extracted from an unbinned maximum likelihood fit; the signal was described with a Crystal Ball function and the background with an exponential.

Charmonia can be produced in primary proton-proton interactions (prompt) and b-hadron decays (non-prompt); the two components were separated performing a simultaneous fit to the invariant mass and the "pseudo-proper decay length" [19], with a function describing the prompt component with a resolution function, the non prompt component with an exponential convolved with a resolution function, and the background with a gaussian plus an exponential.

In Fig. 4 the fits to the mass and pseudo-proper decay length are shown for J/ψ in a p_T, y bin.

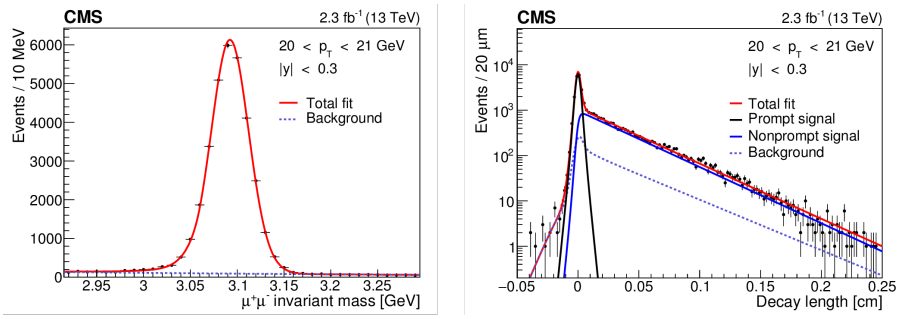

Figure 4: J/ψ fits: mass (left), pseudo-proper decay length (right) [18].

Acceptance has been estimated in a generated event sample by looking at the fraction of generated events passing the selection; in the generation an unpolarized production of quarkonia has been assumed. Efficiency has been estimated with the tag-and-probe method.

Uncertainties related to the signal yield estimation have been evaluated by changing the parameters in the Crystal Ball function, leaving the masses free in the fit and changing the functions for the background. Uncertainties on the non-prompt fraction have been estimated by calculating the decay length from the primary vertex in place of the average collision point, using different functions for the background or changing parameters constraints.

The double-differential cross sections times the dimuon branching fractions vs. p_T for different y bins are shown in Fig. 5; the cross sections times the dimuon branching fractions for the rapidity-integrated range $|y| < 1.2$ are shown in Fig. 6, together with the comparison with the measurements at 7 TeV [20, 21].

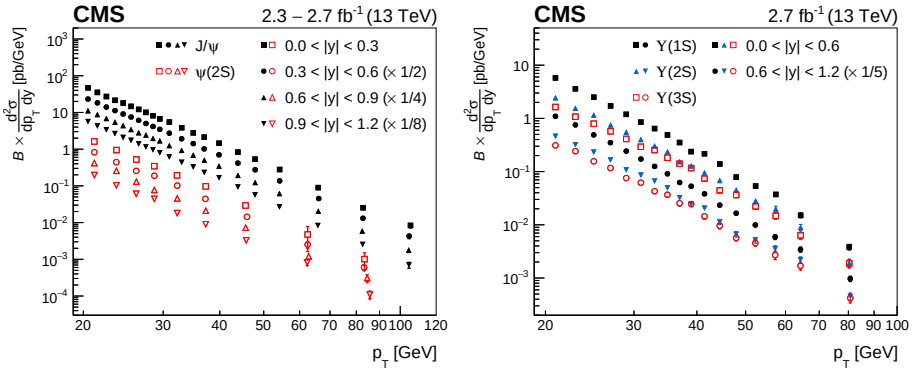

Figure 5: Double-differential cross sections times the dimuon branching fractions vs. y and p_T for charmonium (left) and bottomonium (right) [18].

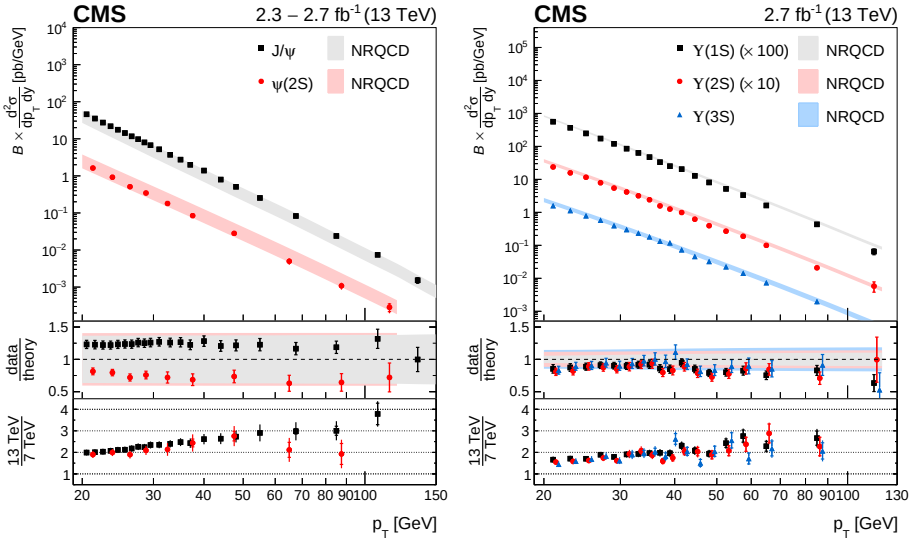

Figure 6: Integrated cross sections vs. p_T for charmonium (left) and bottomonium (right) [18].

Fig. 7 shows the p_T differential cross section times the dimuon branching fractions for $\psi(2S)$ relative to J/ψ and $\Upsilon(1S)$, $\Upsilon(2S)$ relative to $\Upsilon(1S)$.

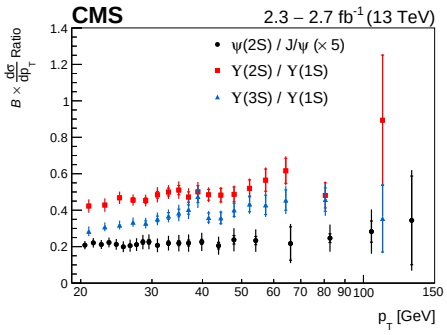

Figure 7: Ratios of the p_T differential cross sections times dimuon branching fractions of charmonium and bottomonium radial excitations to the corresponding ground state for $|y| < 1.2$ [18].

5. Conclusions

The differential cross section for B^+ production at $\sqrt{s} = 13$ TeV has been measured for p_T up to 100 GeV; a reasonable agreement with FONLL calculations and PYTHIA has been found.

The double differential production cross sections at $\sqrt{s} = 13$ TeV for J/ψ, $\psi(2S)$, $\Upsilon(n\mathrm{S})$ with $n = 1,2,3$ has been measured. These results shall contribute to consolidate the underlying hypotheses of NRQCD and provide further input to constrain the theory parameters.

References

[1] CMS Collaboration, J. Inst. **03** (2008) S08004, doi: 10.1088/1748-0221/3/08/S08004

[2] M. Cacciari *et al.*, J. High Energy Phys. **05** (1998) 007, doi: 10.1088/1126-6708/1998/05/007

[3] B.A. Kniehl *et al.*, Phys. Rev. D **77** (2008) 014011, doi: 10.1103/PhysRevD.77.014011

[4] CMS Collaboration, Phys. Lett. B **771** (2017) 435, doi: 10.1016/j.physletb.2017.05.074

[5] CMS Collaboration, Phys. Rev. Lett. **106** (2011) 112001, doi: 10.1103/PhysRevLett.106.112001

[6] M. Cacciari *et al.*, J. High Energy Phys. **03** (2001) 006, doi: 10.1088/1126-6708/2001/03/006

[7] M. Cacciari *et al.*, J. High Energy Phys. **10** (2012) 137, doi: 10.1007/JHEP10(2012)137

[8] T. Sjöstrand *et al.*, Comp. Phys. Comm. **178** (2008) 852, doi: 10.1016/j.cpc.2008.01.036

[9] M. Cacciari *et al.*, arXiv:1507.06197 (2015)

[10] G.T. Bodwin *et al.*, Phys. Rev. D **51** (1995) 1125, doi: 10.1103/PhysRevD.51.1125

[11] G.T. Bodwin *et al.*, Phys. Rev. D **55** (1997) 5853, doi: 10.1103/PhysRevD.55.5853

[12] P. Cho and A.K. Leibovich, Phys. Rev. D **53** (1996) 150, doi: 10.1103/PhysRevD.53.150

[13] P. Cho and A.K. Leibovich, Phys. Rev. D **53** (1996) 6203, doi: 10.1103/PhysRevD.53.6203

[14] B. Gong *et al.*, Phys. Rev. Lett. **112** (2014) 032001, doi: 10.1103/PhysRevLett.112.032001

[15] Z.-B. Kang *et al.*, Phys. Rev. D **91** (2015) 014030, doi: 10.1103/PhysRevD.91.014030

[16] P. Faccioli *et al.*, Phys. Lett. B **736** (2014) 98, doi: 10.1016/j.physletb.2014.07.006

[17] G.T. Bodwin *et al.*, Phys. Rev. Lett. **113** (2014) 022001, doi: 10.1103/PhysRevLett.113.022001

[18] CMS Collaboration, Phys. Lett. B **780** (2018) 251, doi: 10.1016/j.physletb.2018.02.033

[19] CMS Collaboration, Eur. Phys. J. C **71** (2011) 1575, doi: 10.1140/epjc/s10052-011-1575-8

[20] CMS Collaboration, Phys. Rev. Lett. **114** (2015) 191802, doi: 10.1103/PhysRevLett.114.191802

[21] CMS Collaboration, Phys. Lett. B **749** (2015) 14, doi: 10.1016/j.physletb.2015.07.037